Journal of Molecular Graphics and Modelling 29 (2010) 102–114

Contents lists available at ScienceDirect

Journal of Molecular Graphics and Modelling

journal homepage: www.elsevier.com/locate/JMGM

Understanding the stereospecific interactions of 3-deoxyphosphatidylinositol derivatives with the PTEN phosphatase domain

Qin Wang, Yang Wei, Madhusoodanan Mottamal, Mary F. Roberts, Goran Krilov*

Department of Chemistry, Boston College, Merkert Chemistry Center, 2609 Beacon Street, Chestnut Hill, MA 02467, United States

ARTICLE INFO

Article history:
Received 12 March 2010
Accepted 7 May 2010
Available online 20 May 2010

Keywords:
PTEN
Apoptosis
PI3K/AKT
Molecular dynamics
Cancer
Phosphatidylinositol

ABSTRACT

PTEN is an important control element of PI3K/AKT signaling involved in controlling the processes of embryonic development, cell migration and apoptosis. While its dysfunction is implicated in a large fraction of cancers, PTEN activity in the same pathway may also contribute to metabolic syndromes such as diabetes. In those cases, selective inhibitors of PTEN may be useful. A new class of chiral PTEN inhibitors based on the 3-deoxy-phosphatidylinositol derivatives was recently identified (Wang et al. [17]). However, lack of detailed understanding of protein–ligand interactions has hampered efforts to develop effective agonists or antagonists of PTEN. Here, we use computational modeling to characterize the interactions of the diverse 3-deoxyphosphatidylinositol inhibitors with the PTEN protein. We show that, while each of the compounds binds with the inositol headgroup inserting into the proposed active site of the PTEN phosphatase domain, hydrogen bonding restrictions lead to distinct binding geometries for ligand pairs of opposite chirality. We furthermore demonstrate that the binding modes differ primarily in the orientation of acyl tails of the ligands and that the activity of the compounds is primarily controlled by the effectiveness of tail–protein contacts. These findings are confirmed by binding affinity calculations which are in good agreement with experiment. Finally, we show that while more potent D-series ligands bind in a manner similar to that of the native substrate, an alternate hydrophobic pocket suitable for binding the opposite chirality L-series inhibitors exists, offering the possibility of designing highly selective PTEN-targeting compounds.

1. Introduction

PTEN (phosphatase and tensin homologue deleted on chromosome 10) is a dual-function inositol lipid and protein phosphatase which plays a crucial role in regulating the phosphatidylinositol-3-kinase (PI3K)/AKT cellular signaling pathway [1–5]. The latter controls various cellular responses, such as cell survival, proliferation and motility and is found to be upregulated in numerous cancer cell lines and solid tumors [6–9]. PTEN functions as a tumor suppressor by antagonizing PI3K signaling through selective dephosphorylation at the 3′ position of the inositol ring of phosphatidylinositol 3,4,5-triphosphate [PI(3,4,5)P_3] second messengers produced by PI3K, which prevents downstream activation of pro-survival enzymes such as AKT [10]. Mutations of PTEN resulting in the deregulation of this pathway were found to enhance tumor growth in some 30% of human cancers [11]. While emphasis has been on dysfunction of PTEN in cancer biology, PTEN activity in the PI3K/AKT pathway may also contribute to metabolic syndromes such as diabetes, where evidence suggests that AKT may be inhibited [12]. In support of this, animals with deletions of PTEN, while they may have other problems, show hypersensitivity to insulin [13–15]. These interconnections suggest that selective inhibition of PTEN may be useful under some circumstances [16].

D-3-Deoxy-phosphatidylinositol (D-3-deoxy-PI) molecules have been developed as antitumor compounds that are supposed to bind to the PH domain (Pleckstrin Homology domain) of AKT and prevent its translocation to the plasma membrane for phosphorylation and activation. They may also interact with other enzymes that bind inositol moieties, PTEN, being one candidate. A recent study [17] used stereochemical changes and systematic deoxygenation to probe the cytotoxicity of soluble 3-deoxy-dioctanoylphosphatidylinositol (3-deoxy-diC_8PI) derivatives (Scheme 1) [18–20]. PTEN inhibition was also examined, and a very intriguing pattern was observed. Monomeric D-3-deoxy-diC_8PI (**2** in Scheme 1) was a good PTEN inhibitor with affinity comparable to the monomeric substrate D-dioctanoylphosphatidylinoitol-3-phosphate (**S** in Scheme 1), while the L-3-deoxy-diC_8PI (**1**) had little effect on the enzyme. However, further deoxygenation of the D-inositol ring weakened inhibition, but significantly strengthened the inhibition potency of the L-inositol series.

* Corresponding author. Present address: Schrödinger, Inc., 120 West 45th Street, 17th Floor, New York, NY 10036, United States. Tel.: +1 212 548 2335.
E-mail address: goran.krilov@schrodinger.com (G. Krilov).

1093-3263/$ – see front matter © 2010 Elsevier Inc. All rights reserved.
doi:10.1016/j.jmgm.2010.05.004

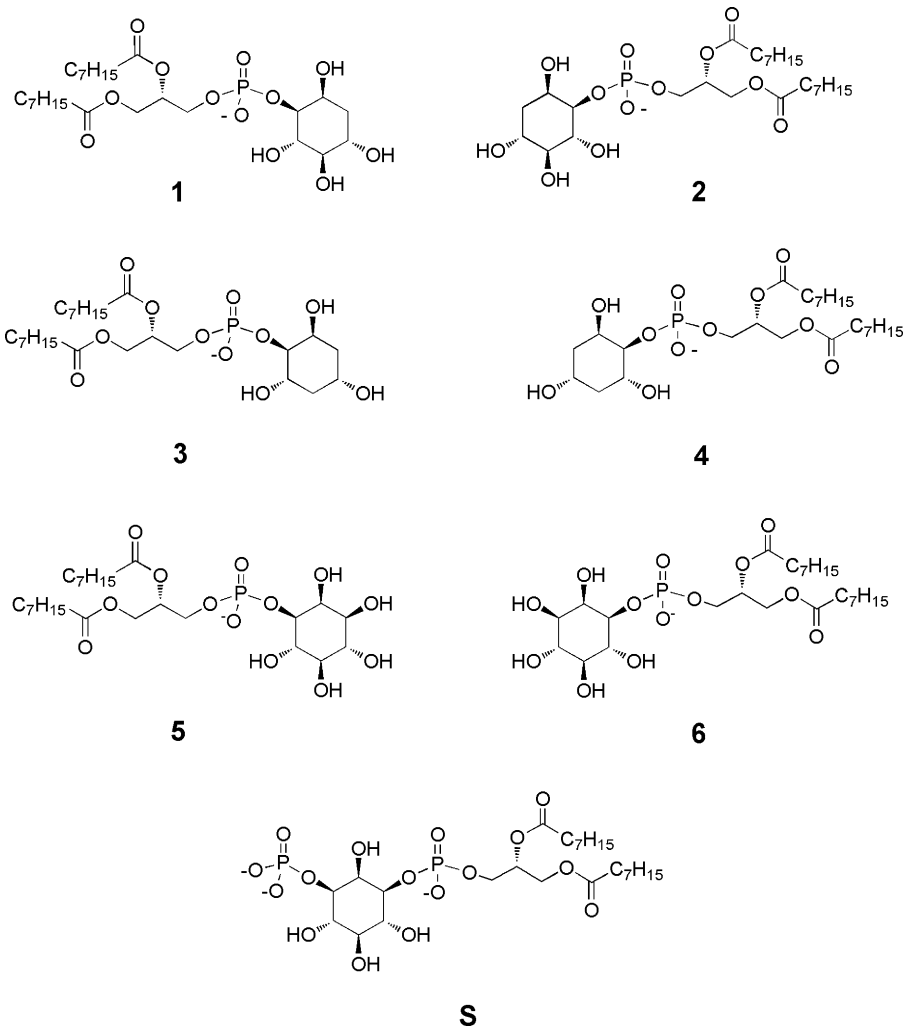

Scheme 1. The substrate analog diC$_8$PI(3)P (**S**) and the six 3-deoxy-dioctanoylphosphatidyl inositol (3-deoxy-diC$_8$PI) inhibitors.

The differences in inhibition among the different deoxy-diC$_8$PI compounds might prove useful in fine-tuning molecules that select for or against binding to PTEN. Although a crystal structure of PTEN exists [21], only tartrate and not a more substrate-like molecule occupied the active site. The PTEN active site is rich in charged residues that could interact differently with modified inositol compounds. Limited modeling suggests how I(1,3,4,5)P$_4$ might bind in the PTEN active site, but there is no structure to confirm this arrangement, or to suggest where any hydrophobic segments, which are present in all the optimized 3-deoxy-PI inhibitors [22–24], might bind. Given its extreme functional importance, understanding how different substrate-like molecules bind to PTEN is critical.

The 403 amino acid sequence comprising the minimum catalytic unit of PTEN consists of the Ca^{2+} independent membrane-binding C2 domain, and the phosphatase domain [21]. The latter serves as the catalytic domain and contains the active site characterized by a seven residue motif common to dual-specificity protein phosphatases supplemented by two unique positively charged lysine residues at positions 125 and 128, the role of which may be to provide binding specificity towards negatively charged PI substrates. The affinity for acidic membranes or phospholipid vesicles is believed to be further enhanced through interactions of a basic lipid binding motif at the N-terminus of the phosphatase domain with PI(4,5)P$_2$ [25,26].

This work describes the use of molecular dynamics simulations together with quantum mechanical and free energy calculations to characterize the interactions between the series of D- and L-3-deoxy-diC$_8$PI monomers shown in Scheme 1 and the phosphatase domain of PTEN, and to determine the preferred binding modes. We find that different members of the series, including enantiomeric pairs, bind with distinct, well-defined geometries which differ not only in the pattern of hydrogen bonds formed between the substituted inositol head groups and the PTEN active site residues, but also in the relative orientation of the lipid tails with respect to the protein. We next show that the degree of favorable tail–protein interactions correlates well with both the variations in experimentally measured inhibition constants among complexes, as well as the computed relative binding free energies, indicating that the PI–protein interaction is dominated by these hydrophobic terms at concentrations far below the CMC (concentrations that would exist in cells treated with these soluble deoxy-diC$_8$PI compounds). Furthermore, we present an analysis of protein dynamics that indicates the binding of good inhibitors generally leads to suppression of fluctuations, whereas complexes with poor inhibitors show increased flexibility and reduced structural stability. In addition, our quantum mechanical calculations show substantial differences in the charge distribution of the inositol ring between the free monomer in an aqueous solution and the protein complex, which may also provide insight into

the substrate specificity of the PTEN catalyzed dephosphorylation.

2. Methods

2.1. Initial structure preparation

The structural models for the PTEN–PI complexes were constructed by incorporating both crystallographic and biochemical data. The initial configurations of PTEN were obtained from the X-ray structure of the protein with the tartrate bound to the active site (PDB code 1D5R). The C2 domain of PTEN protein was truncated and the tartrate ion was deleted from the active site located on the phosphatase domain. Hydrogen atoms were added to the proteins as necessary and the protonation states of ionizable residues were assigned according to the pK_a based on pH 7.0 using the GROMACS package [27–29]. The structures of phosphatidylinositol ligands were built using the MAESTRO package [30]. Each molecule was then soaked with a box of pre-equilibrated water. Overlapping solvent molecules were removed and an appropriate number of counter-ions were added to maintain charge neutrality. In each case, the system was equilibrated via energy minimization to remove bad contacts, followed by 2 ns molecular dynamics simulation to explore the ligand conformational space. The most populated conformations were identified for use as input for the docking calculations.

2.2. Docking calculations

Docking calculations were performed using the genetic algorithm implemented in the GOLD package with full ligand flexibility. The positions of the residues within 5 Å of the co-crystallized tartrate were used to delineate the target binding site with the deoxy-diC_8PI ligands. Multiple ligand conformations were then docked into this designated PTEN active site and the highest scoring poses were retained and used to generate the starting structures of the 3-deoxy-diC_8PI–PTEN complexes for molecular dynamics simulations.

2.3. Molecular dynamics simulations

All molecular dynamics (MD) simulations were performed with the GROMACS 3.0 package. The ligand and protein interactions were modeled using the OPLS-AA 2001 force field [31,32], and the TIP3P model [33] was used for water. Particle-mesh Ewald method [34] with a grid spacing of 0.8 Å combined with a fourth order B-spline interpolation was used for long-range electrostatics. Short range electrostatic and Van der Waals interactions were truncated smoothly at 10.0 Å via a potential shift. Nose–Hoover thermostats [35] were used to maintain constant temperature, and pressure was controlled using the Berendsen barostat [36]. The lengths of all bonds with hydrogen were constrained using the LINCS algorithm, and the equations of motion were integrated via the leapfrog algorithm with a 2 fs time step.

In each case, the docked ligand–protein complex was placed in an orthorhombic cell, with size adjusted to maintain a 10 Å buffer between the protein and cell boundary, and soaked with pre-equilibrated box of water. All overlapping solvent molecules were removed, and an appropriate number of counterions added to maintain charge neutrality. The solvated complexes were then equilibrated according to the following scheme. A 2000 step steepest descent energy minimization was performed to remove bad contacts. The system was then gradually heated to room temperature (300 K) over 100 ps with the positions of all heavy atoms restrained, followed by a 300 ps simulation at constant NPT of 1 atm and 300 K. A second 300 ps simulation was then performed under the same conditions with only the positions of the ligand heavy atoms and the α-carbons of the protein restrained. Finally, a 2000 ps simulation was performed at constant NVT with positions of all protein heavy atoms restrained. Following equilibration, all restraints were removed, and the trajectory was evolved for a further 2000 ps. Configurations were saved in 4 ps intervals and this data was used for subsequent analysis.

2.4. MM-GBSA calculations

The relative binding free energies of the ligands were estimated using the Molecular Mechanics-Generalized Born and Solvent Accessibility (MM-GBSA) method, where the binding free energy is decomposed into:

$$\Delta G_{\text{bind}} = \Delta G_{\text{gas}} + \Delta_{\text{sol}} G_{\text{complex}} - \Delta_{\text{sol}} G_{\text{ligand}} - \Delta_{\text{sol}} G_{\text{receptor}} \quad (1)$$

Assuming no significant volume change upon ligand binding, the gas phase term is given by

$$\Delta G_{\text{gas}} = \Delta U_{\text{ele}} + \Delta U_{\text{vdw}} + \Delta U_{\text{conf}} \quad (2)$$

which includes contributions from electrostatic (ΔU_{ele}) and non-polar (ΔU_{vdw}) ligand–receptor interactions, as well as the strain energy due to conformational reorganization of the ligand upon binding (ΔU_{conf}), all of which were computed from OPLS-AA 2001 force field terms. The remaining three terms are the solvation contributions,

$$\Delta_{\text{sol}} G = \Delta G_{\text{GB}} + \Delta G_{\text{np}} \quad (3)$$

which consists of the electrostatic term (ΔG_{GB}) due to solvent polarization and the non-polar cavity term (ΔG_{np}). The former is computed via the surface generalized Born method (SGB) [37], and the latter is estimated from the change in the solvent-accessible surface area (SASA) by

$$\Delta G_{\text{np}} = \gamma \Delta(\text{SASA}) \quad (4)$$

where $\gamma = 0.005$ kcal/(mol Å^2) is the microscopic surface tension coefficient. All calculations were performed using the MM-GBSA module of the PRIME package [38]. The reparameterization of ligand atomic partial charges was accomplished via an ESP fit to the quantum mechanical charge distribution for the free ligands in a Poisson–Boltzmann implicit solvent. The latter was obtained from a density functional theory (DFT) calculation with the B3LYP functional and the 6-31G** basis set, using the JAGUAR package [39].

2.5. Overexpression and purification of wild type PTEN

The pET28a PTEN plasmid construction has been described previously [40]. The plasmid was transformed into *E. coli* BL21 (DE3)-RIL cells (Stratagene) and the cells were grown at 37 °C until O.D.$_{600}$ reached 0.8. Protein expression was induced with 0.4 mM isopropyl-β-D-thiogalactoside and the cultures were incubated at 16 °C for 20 h. Cells were harvested by centrifugation and stored at −20° until needed. His$_6$-tagged PTEN was purified from the cell extracts using a Ni-NTA agarose column according to the manufacturer's protocol (Qiagen) with minor modifications. The purification process was carried out at 4 °C with 10 mM β-mercaptoethanol added to all buffers. Pure protein fractions (as judged by SDS-PAGE) were combined and dialyzed against 100 mM Tris–HCl, 1 mM DTT, pH 8.0. Protein concentration was determined by UV absorbance as well as Lowry assay [41].

2.6. Mutagenesis and purification of PTEN single mutants (R47G, R47W, R47L and R47K)

The plasmids for production of PTEN single mutant proteins (R47G, R47W, R47L and R47K) were constructed using

the QuikChange Site-Directed Mutagenesis Kit (Stratagene) with the pET28a PTEN plasmid as the template. The plasmids were sequenced at Genewiz to confirm the presence of the desired mutation. Overexpression and purification of the mutant proteins were the same as for the wild type protein.

2.7. PTEN kinetics

The PTEN phosphatase assay to quantify the release of inorganic phosphate from PI(3)P substrates has been described previously [17]. In this case, the substrate was 0.1 mM dipalmitoyl-PI(3)P (obtained from Echelon) presented to the enzyme either in Triton X-100 micelles or in large unilamellar vesicles with POPC. For the mixed micelle assay, the substrate was mixed with Triton X-100 at a molar ratio of 1:4 dipalmitoyl-PI(3)P/Triton X-100 dissolved in 100 mM Tris–HCl, pH 8.0. For the vesicle system, POPC in chloroform was dried under a stream of nitrogen and lyophilized overnight. The POPC film was mixed with D-diC$_{16}$PI(3)P at a molar ratio of 9:1, then resuspended in 100 mM Tris–HCl, pH 8.0 and vortexed. The resulting multilamellar vesicle solution was extruded through a 0.1 μm polycarbonate membrane to form LUVs with an average diameter of 1000 Å. Both types of assays were carried out in 200 μL buffer (100 mM Tris–HCl, pH 8.0, 2 mM EDTA, and 10 mM DTT) at 37 °C and incubation of the enzyme for 20 or 40 min. Malachite green reagent was added to quench the reaction. Most of the assays are done at least in duplicate.

2.8. Phosphatase assay comparing PTEN with Arg47 mutant proteins

The activity of PTEN with substitutions for Arg47 was determined by the same colorimetric phosphatase assay [17] using 0.5 mM short-chain D-diC$_8$PI(3)P as the substrate in the absence or presence of 0.1 mM L-3,5-dideoxy-diC$_8$PI. The assays were carried out in 50 μL assay buffer (100 mM Tris–HCl, pH 8.0, 2 mM EDTA, and 10 mM DTT) at 37 °C. The amount of the protein added and the reaction time were adjusted to hydrolyze ~5% of the substrate. Most of the assays were done in duplicate.

3. Results and discussion

3.1. Building the initial structures of the PI–PTEN complexes

No high-resolution experimental structures of PTEN in complex with either the native substrate, the diC$_8$PI(3)P substrate analog, or any of the 3-deoxy-PI derivatives have been determined. However, a high-resolution structure of the PTEN catalytic unit with a tartrate ion bound to the phosphatase active site has been solved by Lee et al. [21]. Using the PTEN/tartrate structure as a starting point, the initial structures of the complexes were built by truncating the C2 domain and deleting the co-crystallized tartrate molecule. The substrate analog diC$_8$PI(3)P and each of the six 3-deoxy-diC$_8$PI inhibitors shown in Scheme 1 were then docked into the site formerly occupied by the tartrate using a fully flexible

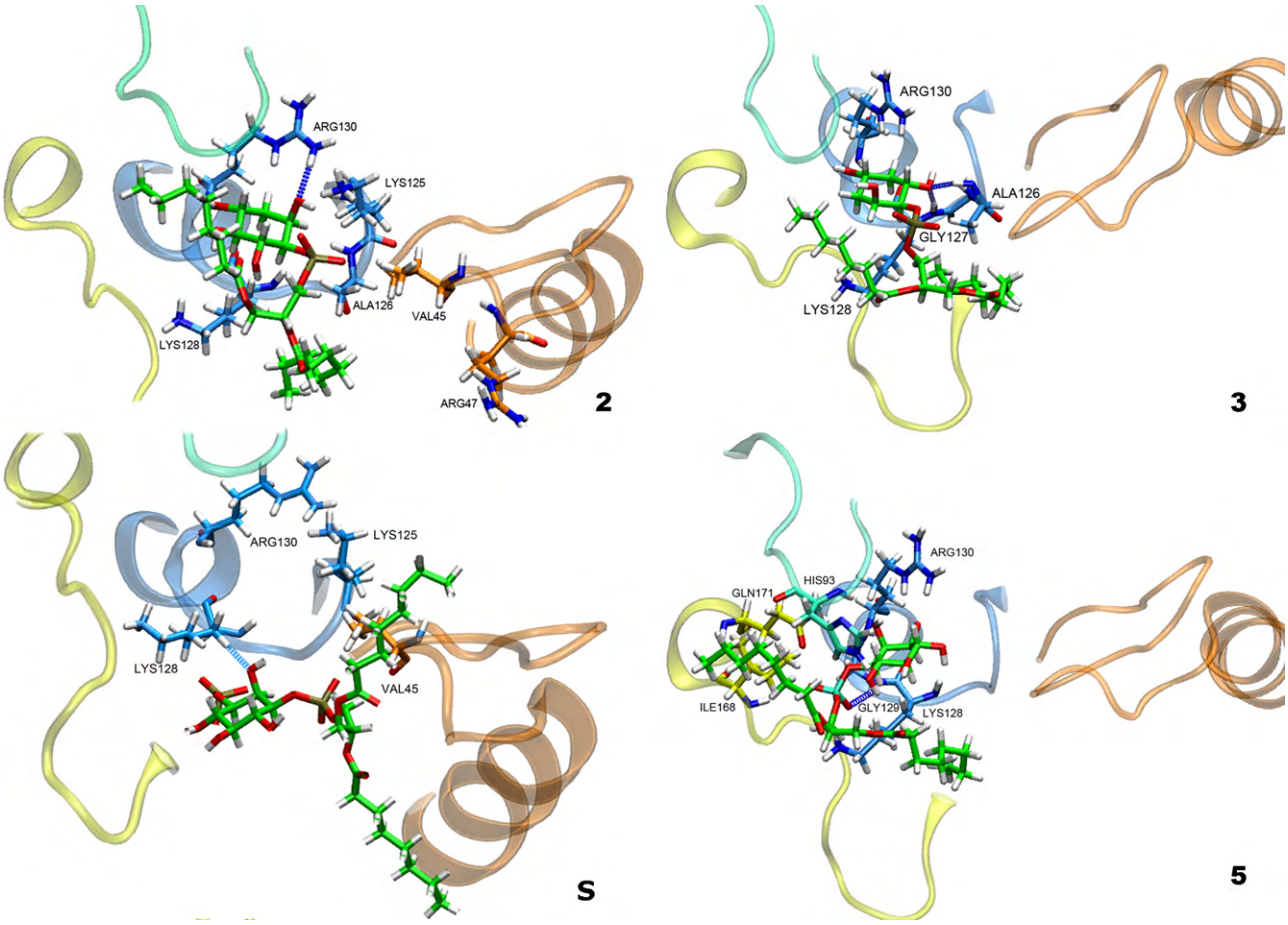

Fig. 1. Initial structures of the PTEN phosphatase domain complexes with compounds **2**, **3** and **5**, and the substrate analog **S**, prepared by docking the ligands into the tartrate binding site. The ligands (green) and adjacent protein residues are shown as sticks and the protein backbone as ribbons. Important ligand–protein hydrogen bonds are shown as dark blue dashed lines.

ligand–rigid receptor model. The genetic algorithm implemented in the GOLD program [42] was used to search through binding poses which were ranked using the GOLD scoring function. The highest scoring pose for each ligand–protein pair was then selected as the starting configuration for further analysis. In Fig. 1 we show the structures of complexes **S**, **2**, **3** and **5** prepared in this fashion.

In each case we find that the inositol head group binds into the pocket previously occupied by the negatively charged tartrate, allowing favorable hydrogen bonds to be formed between the active site residues, and the inositol hydroxyls and phosphates of the ligands. However, the specific pattern of hydrogen bonds was found to vary among ligands (Fig. 1). For example, the most potent inhibitor, **2**, was found to form but a single hydrogen bond between 2-hydroxyl and Arg130, while **5**, the least potent inhibitor, was found to form one hydrogen bond between the phosphate and Gly129. Conversely, no significant amount of hydrogen bonds were predicted for the bound substrate analog **S**. On the other hand, the acyl tails of the ligands were largely predicted to extend into the solvent, forming few protein contacts, which appears to be less than optimal arrangement for these highly lipophilic groups. A similar result was obtained for the remaining three 3-deoxy-diC_8PI inhibitors, with the structures of the highest-ranked poses given in Fig. S1 of the Supplementary Information.

The challenges in accurately predicting the binding geometries of the PI derivatives stem from well-known limitations [42] of the GOLD genetic search algorithms which are designed to first identify hydrogen bonding networks, and are likely to fail if the ligand is large or highly flexible. Moreover, while the GOLD scoring function contains a term that describes dispersion interactions, it fails to adequately take into account desolvation and therefore underestimates the hydrophobic effect, which is expected to play a prominent role in determining the thermodynamically favorable conformation of the acyl tails of the ligands. Hence, a more accurate approach which includes explicit treatment of solvation and takes into account the dynamic nature of the PTEN–PI complexes is needed in order to probe the thermodynamics of binding.

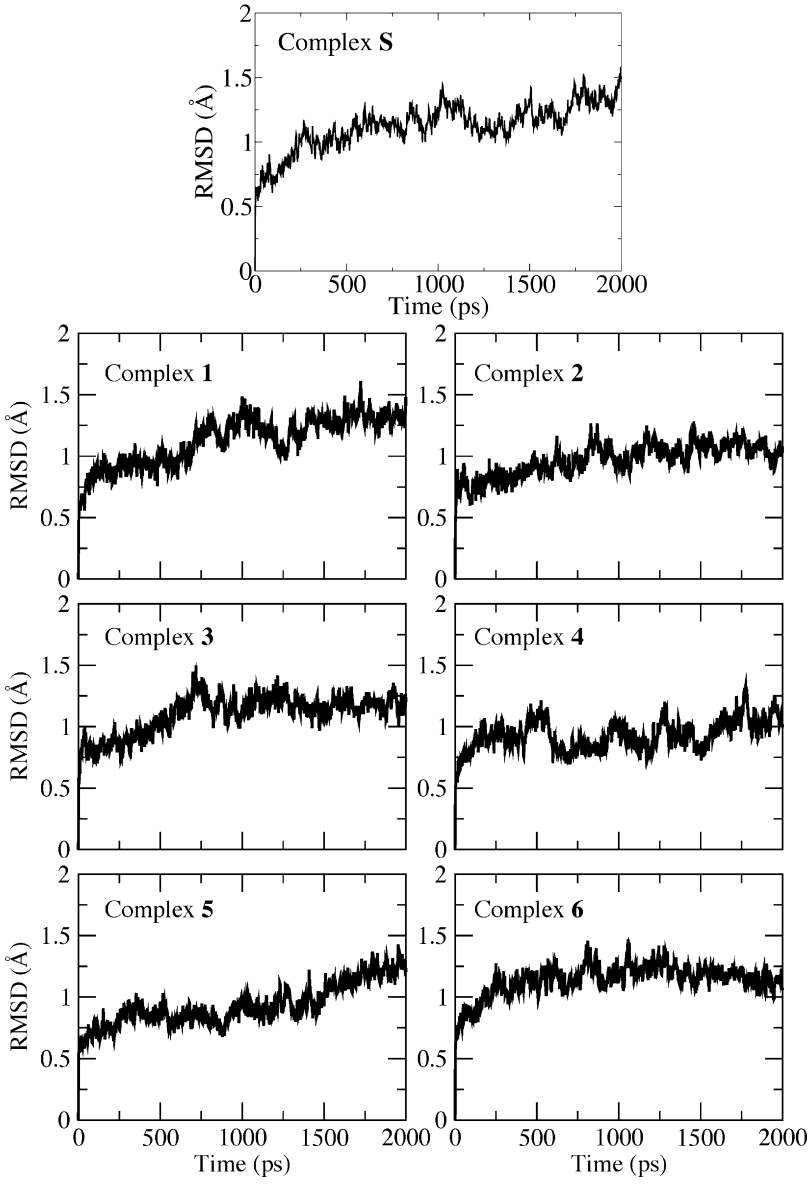

Fig. 2. Root mean square deviations of the protein backbone atoms from initial equilibrated conformations in complex with the substrate analog (**S**) and ligands **1**–**6** shown as a function of time. All complexes were found to be relatively stable throughout the simulation.

3.2. Refinement of the binding mode geometry and stability of simulations

In order to refine the structures of the complexes, and improve the accuracy of the predicted binding geometries for the deoxy-PI inhibitors, the initial structures generated by docking were immersed in a periodic box of aqueous solvent molecules. Following a standard equilibration procedure, each system was evolved for 4 ns via constant NVT molecular dynamics. The ensemble of structures collected during the final 2 ns of the run for each of the seven complexes was used for subsequent analysis. To ascertain the stability of the ligand protein complexes in MD simulations, we analyzed the root mean squared deviation (RMSD) of the protein backbone over the production portion of the simulation from the initial equilibrated structures (Fig. 2).

In all cases the profiles are reasonably flat, with the RMSD values remaining below 1.5 Å throughout the simulation, indicating that the PTEN phosphatase domain maintains structural integrity in all complexes. A slight increase observable in RMSD profiles for the complexes with the substrate and **1** is mainly due to increased fluctuations in protein termini, however the region surrounding the binding site is quite well preserved.

A cluster analysis of the full set of sampled conformations was performed for each of the ligands in order to characterize the binding modes. The ligand conformations were found to group in a single cluster with an RMSD among all members of a cluster less than 1.1 Å, indicating a single, well-defined ligand binding mode for each of the complexes. In Fig. 3 we show the binding geometries of the representative central structures of the clusters for complexes with compounds **2**, **3**, **5** and **S**, along with the principal ligand–protein hydrogen bonds, where a given hydrogen bond was deemed significant if present in at least 10% of sampled conformations.

It is interesting to note that the hydrogen bond patterns observed in MD simulations are in most cases substantially different from those predicted by docking calculations. For example, the complex with compound **2** exhibits hydrogen bonding between inositol hydroxyls and Arg130 and Ala126, while no significant interactions were observed with Arg126 in the docked structure. On the other hand, complex **5** shows that the hydrogen bond between Gly129 and the inositol phosphate in the docked structure has been replaced by a strong hydrogen-bonded salt bridge with Lys128 (found in 69% of the conformations) and further augmented by hydrogen bonding to His93, with several additional hydrogen bonds forming between inositol hydroxyls and Arg130. Hence, even though **5** is a poorer inhibitor than **2**, the L-series ligand appears to be able to establish a more favorable hydrogen bonding network within the PTEN active site. This finding is encouraging, as it suggests a new avenue for the design of L-inositol based inhibitors with high PTEN specificity, as such compounds would be less likely to interact effectively with PI3K and PI-PLC enzymes, which bind D-inositol based second messengers. An interesting change in the hydrogen bonding pattern is observed in complex **S**, with significant amount of hydrogen bond interactions involved

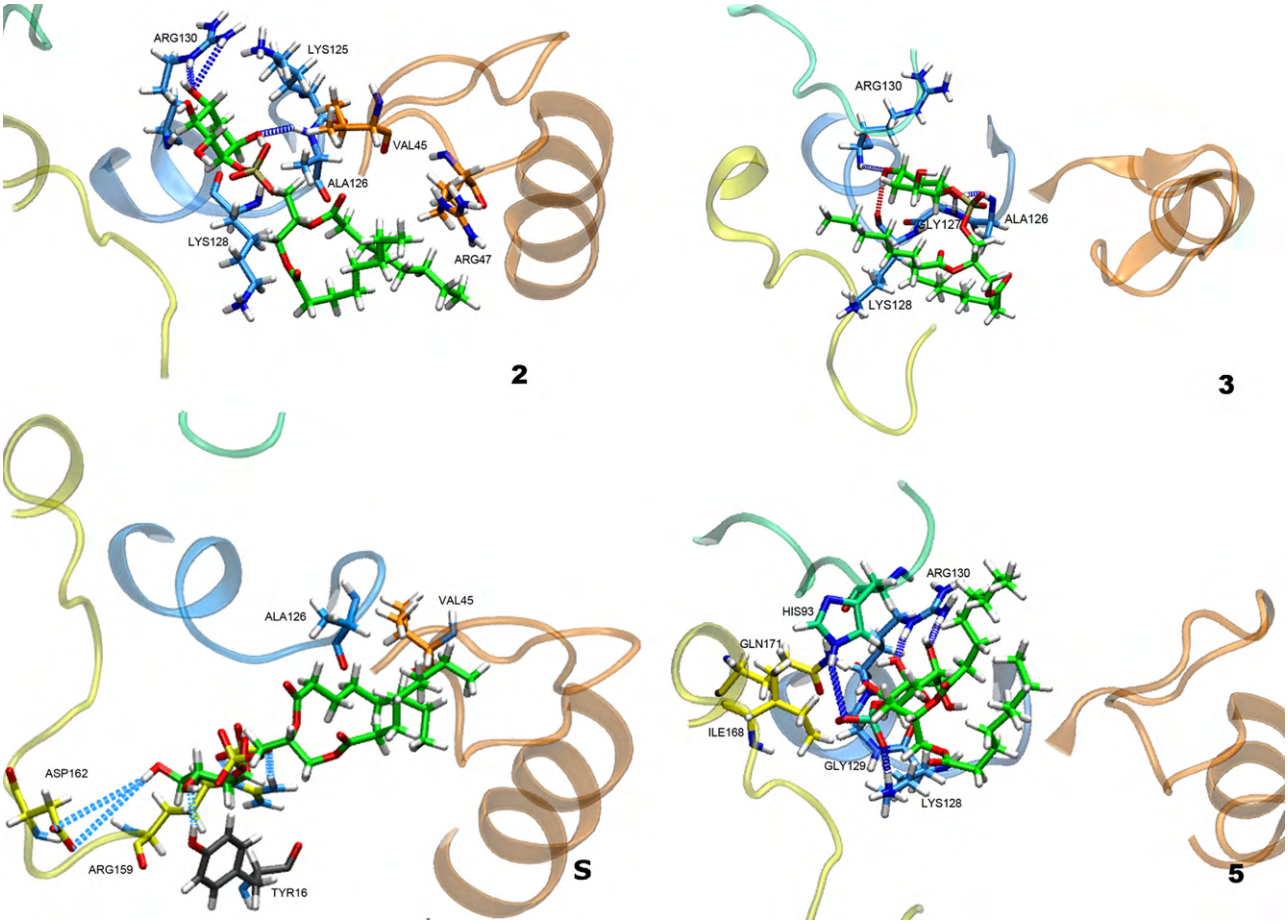

Fig. 3. Median structures of the PTEN phosphatase domain complexes with compounds **2**, **3** and **5**, and the substrate analog **S**, obtained by clustering configurations collected from a 2 ns MD simulation. The ligands (green) and adjacent protein residues are shown as sticks and the protein backbone as ribbons. Important ligand–protein hydrogen bonds are shown as dark blue dashed lines. Note the difference in tail orientation between the D-series (**2** and **S**) and L-series (**3** and **5**) ligands. (For interpretation of the references to color in this figure legend, the reader is referred to the web version of the article.)

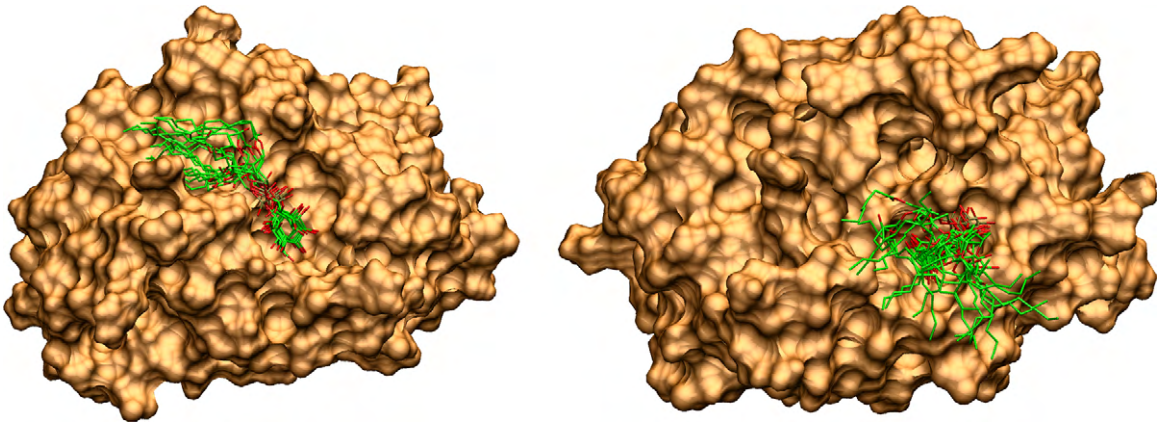

Fig. 4. Representative snapshots of the conformations of compound **2** (left) and compound **5** (right) bound to the active site of the PTEN phosphatase domain from a 2 ns MD simulation. The ligands are shown as sticks, while the accessible protein surface is shown in tan. The difference of the ligand tail flexibility in the two complexes is clearly visible.

in stabilization of the bound complex. The substrate was found to be stabilized in the binding site by a set of strong and persistent hydrogen bonds between inositol hydroxyls and phosphate group with Tyr16, Arg159 and Asp 162. The binding geometries and hydrogen bonds of the remaining ligands are given in Fig. S2 of the Supporting Information.

In order to understand these patterns and their relationship to inhibitor potency, it is important to examine the role of lipophilic acyl tails in controlling the binding geometry of 3-deoxy-diC_8PI inhibitors. Examination of the MD trajectory animations provided as Supporting Information, and snapshots of the ligand conformations shown in Fig. 3, reveals that in the PTEN complex with **S**, substrate lipophilic tails pack against the pβ_2–α_1 loop, making hydrophobic contacts with Val45, Arg47 and Tyr46. The D-series ligand **2**, which is of the same chirality as the substrate, exhibits a similar tail conformation, however changes in the inositol ring orientation due to lack of the bulky phosphate group at the 3-position allow better positioning of the tails within the cleft formed by the pβ_2–α_1 loop and the P loop, as well as facilitating additional hydrophobic contacts with Gln17, Asp22, Leu23 and Asp24 of the nearby N-terminus loop. One tail of ligand **2** remains firmly in place throughout the simulation, while the other shows only minor excursions from the cleft region. Hence, it would seem that the pβ_2–α_1-P cleft provides an important contribution to high inhibition potency of D-3-deoxy-diC_8PI ligands by providing a favorable hydrophobic binding pocket for the lipophilic acyl tails. The presence of such a pocket in close proximity to the PTEN active site presents an attractive target for the design of novel dual binding site amphiphilic inhibitors. On the other hand, in order to maintain the favorable hydrogen bonding interactions with the polar active site residues, the opposite chirality of the inositol ring of the L-series compound **5** forces the inhibitor to assume a binding geometry with acyl tails oriented away from the hydrophobic binding sites along the pβ_2–α_1-P loop cleft. This leaves the lipophilic tails exposed to the solvent, and unable to interact effectively with the protein, which is evident in large amplitude motions characterizing the flipping of the tails from loose association with the His93 of the WPD loop to that with Val45 of the pβ_2–α_1 (see Movie M5 provided in Supporting Information). This is illustrated in Fig. 4 which shows representative snapshots of the ligand conformations in relationship to the protein surface.

The distributions of tail geometries of the remaining D-series and L-series ligands parallel that of **2** and **5**, respectively, and the animations of the corresponding trajectories are provided as Supporting Information. Among the latter, **3** – the only good inhibitor of the L-series 3-deoxy-diC_8PIs – also displays strong association of its lipophilic tails with the protein akin to D-series ligands. However, instead of interactions with the pβ_2–α_1–P loop cleft, one of the tails of **3** is found to firmly insert into a deep pocket framed by Tyr16, Arg47, Ala126, Gly127, Lys128, Thr160 and Gly165, while the other associates with His93 and Leu168, both on the opposite side of the active site, indicating a binding mechanism distinct from that of the substrate and the D-series ligands. The above results suggest a relationship between the inhibition potency of the PI compounds and the ability of the ligands to achieve binding geometries permitting favorable tail–protein interactions. It is therefore of interest to investigate if a more quantitative correlation can be established. In Table 1 we give the average hydrophobic contacts formed by the two acyl tails of each of the six 3-deoxy-diC_8PI inhibitors and the substrate analog with the protein, as well as the experimental values for IC_{50} according to Wang et al. [17], and in Fig. 5 we plot the former vs. the $-\log[IC_{50}]$. The contact number was arbitrarily defined as a number of ligand tail heavy atoms within 3.5 Å of protein heavy atoms. A high degree of correlation indicates that hydrophobic tail–protein interactions play a significant role in controlling the binding affinity of these PI inhibitors.

Protein flexibility is known to be important in modulating the activity of small molecule substrates and inhibitors. Several groups have proposed that membrane induced structural changes to the flexible PTEN active site may help explain substrate specificity of the dephosphorylation action of the protein. However, flexible behavior is often difficult to ascertain from static structures typically available from experiments. On the other hand, information about protein dynamics is readily available from MD trajectories. To investigate the relationship of the protein flexibility to the inhibition profiles of the 3-deoxy-diC_8PI inhibitors, we analyzed the variations in local mobility of the protein backbone of the seven diC_8PI–PTEN complexes. In Fig. 6 we plot the per-residue root-mean-squared fluctuation (RMSF) of the protein for complexes

Table 1
Average number of contacts between the acyl tails of the C_8PI ligands computed from MD simulations.

Compound	Tail 1	Tail 2	Total	IC_{50}[a] (mM)
1	1.31	0.25	1.56	1.5 ± 0.2
2	1.17	1.88	3.05	0.23 ± 0.03
3	2.06	0.69	2.75	0.38 ± 0.05
4	0.40	0.73	1.13	0.86 ± 0.10
5	0.20	0.24	0.44	>2.5
6	0.97	0.56	1.53	0.43 ± 0.05
S	0.12	0.28	0.40	–[b]

[a] Experimental data and errors as reported in Ref. [17].
[b] The K_m for this substrate was determined to be 0.2 ± 0.07 mM [17].

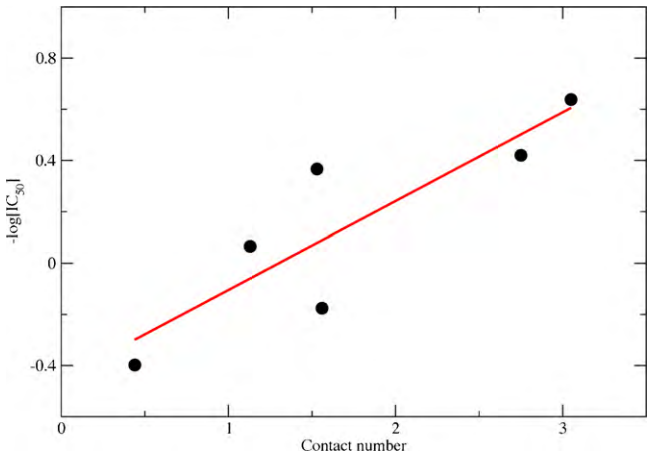

Fig. 5. The average number of contacts (black circle) between acyl tails of the C_8PI ligands plotted against the binding affinities estimated from the experimentally measured IC_{50} values. The red line shows a linear fit with a correlation coefficient $R^2 = 0.757$. (For interpretation of the references to color in this figure legend, the reader is referred to the web version of the article.)

with **2**, **3** and **5**, in comparison to that of the substrate complex.

With the exception of the highly flexible termini, the complexes with both inhibitors **2** and **3** show suppression of mobility relative to the substrate complex in several regions of the PTEN phosphatase chain, in particular parts of the $p\beta_2$–α_1 loop (residues 41–45), the $p\alpha_2$–$p\beta_4$ loop (residues 82–85), the P-loop (residues 125–130) and the TI loop (residues 155–163). Out of these, only the P-loop region includes the active site residues in direct contact with the inositol headgroup, which are more favorable for the dideoxy compound **3**. On the other hand, the inositol head group in the complex with **2** makes comparatively fewer contacts with active site residues, but nonetheless provides a comparable stabilization of this region. This is most likely due to favorable hydrophobic contacts formed by the acyl tails with P-loop Lys128 and Ala126. Good tail–protein contacts are also observed with the N-terminus loop and the $p\beta_2$–$p\alpha_1$ loop described previously, and may explain the observed stabilization of these regions of the protein. Conversely, ligand **5** forms much fewer contacts with the protein chain in these regions since the opposite chirality of the head group forces the tail to orient in a different direction. Moreover, complex **5** shows a significant local destabilization of parts of $p\beta_2$–$p\alpha_1$ loop and the $p\alpha_1$ helix (residues 45–60), and the TI loop (residues 162–164), all of which show a marked increase in flexibility relative to complex **S**. The same protein regions are somewhat less destabilized in the complex with the more potent inhibitor **2**, primarily through hydrophobic interactions with the acyl tails of the latter ligand. In particular, the complex with **3** shows marked stabilization of the $p\beta_2$–$p\alpha_1$ loop (residues 41–48), $p\beta_2$–$p\beta_3$ loop (residue 70–74), parts of the WPD loop (residues 92–94), the $p\alpha_5$ helix (residues 154–159) and the TI loop (residues 160–165), all of which contain residues which enclose the acyl tail of the ligand. Similar trends were observed in the remaining three deoxy-diC_8PI–PTEN complexes, and the data are provided in Fig. S3 of the Supporting Information. These results suggest a correlation between increased inhibition potency of the deoxy-diC_8PI ligands and their ability to stabilize the local protein fluctuations. Although this may appear counterintuitive, since suppression of protein motions would seem to introduce an entropic penalty to complex formation, this is more than compensated by the enthalpic contribution due to improved ligand–protein and protein–protein contacts. A similar effect was observed in our analysis of interactions of small molecule inhibitors with the peptide binding interface of Bcl-X_L [43], as well as by Mancinelli et al. [44] in their studies of the binding of proapoptotic peptides to Bax, and more recently, by Dastidar et al. [45] who investigated the binding of p53 mutants to MDM-2.

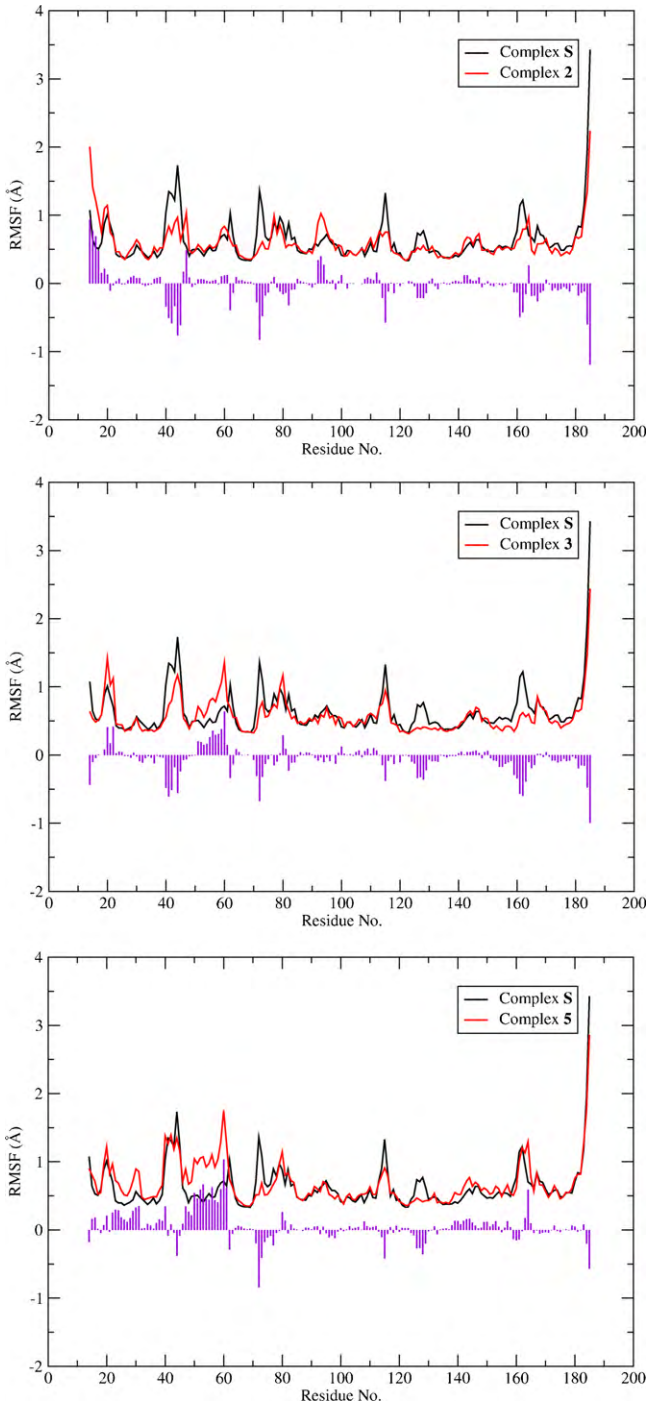

Fig. 6. Average root mean square fluctuations of the backbone atoms for each residue of the PTEN phosphatase domain in complex with ligands **2**, **3** and **5** (red lines) in comparison with the substrate analog complex (black line). The purple bars show the difference in per residue RMSF between the substrate and corresponding inhibitor complex. (For interpretation of the references to color in this figure legend, the reader is referred to the web version of the article.)

3.3. Characterization of binding energetics and key ligand–protein interactions

Kinetic measurements by Wang et al. [17] in the presence of 0.5 mM D-3-deoxy-diC_8PI(3)P substrate have shown median

inhibitory capacity of the six 3-deoxy-diC_8PI compounds in the tenth millimolar to millimolar range with D-series **2** being the most potent (IC_{50} = 0.23 mM) and the L-series **5** the least potent (IC_{50} > 2.5 mM) inhibitor. The IC_{50} values for all six compounds are provided in Table 1. To investigate the binding mechanism of these weak PTEN inhibitors in more detail, we computed the total interaction energy of the ligands with each protein residue. The latter was defined as the sum of electrostatic (Coulomb) and non-polar (Lennard-Jones) interactions of all ligand atoms with the backbone and side chain atoms of a given protein residue. The interaction profiles for the substrate complex, and those with compounds **2**, **3** and **5** are shown in Fig. 7, and for the remaining four ligands in Fig. S4 of Supplementary Information.

In all three cases, electrostatic interactions with active site residues are an important feature. In particular, strong hydrogen bonds between Tyr16, Arg159 and Asp161 and the substrate phosphate, as well as salt bridge with Lys128 are clearly evident in the interaction profile of the PTEN **S** complex. Coulomb interactions with Lys128 and Arg130 are also the most prominent features in the interaction profile of complex **5**, where the former residue forms a hydrogen bonded salt bridge with the phosphate, which is also stabilized by accepting a hydrogen bond from His93, while Arg130 interacts through multiple hydrogen bonds with hydroxyls of the inositol ring. Interestingly, the most potent inhibitor **2** shows the weakest electrostatic interactions among the three. The primary stabilization of the inositol in complex **2** is via a hydrogen bonded salt bridge between the Arg130 amine and the 4-hydroxyl, a weaker hydrogen bond between the backbone amine of Ala126 and the axial 2-hydroxyl, as well as polar interactions with the nearby Lys125. In addition, internal hydrogen bonds between the equatorial 2-inositol and 6-inositol hydroxyls and the phosphate oxygen help stabilize the binding mode. However, the high binding affinity of D-3-deoxy-diC_8PI can be understood by examining the non-polar interactions. The interaction energy of complex **2** shows numerous favorable non-polar contributions, mainly due to tight hydrophobic association of the acyl tails with residues lining the pβ_2–α_1-P cleft, including residues 45, 47, 128, 126 and 24. Additional stabilization to the tails is provided by the occasional salt bridge between the positively charged Lys128 amine and the acyl oxygen. Similar hydrophobic interactions with the residues of the pβ_2–α_1-P cleft are observed for the substrate complex, but the interactions are overall weaker, since the bulky phosphate prevents the proper positioning of the inositol in the active site precluding the formation of favorable hydrophobic contacts between the tails and the N-terminus loop residues of PTEN. On the other hand, hydrogen bonding restrictions within the active site require the acyl tails of the opposite chirality ligand **5** to be oriented away from the pβ_2–α_1-P cleft. While this configuration allows for very favorable electrostatic interaction with the head group, the tails are forced to occupy mostly a broad, solvent exposed region between pβ_2-α_1 and WPD loop. The tails are observed to be quite mobile throughout the simulations, occasionally associating loosely with His93 of WPD, and Ile168. This arrangement leaves a large lipophilic surface exposed to water, and the resulting hydrophobic solvation penalty is probably the principal factor contributing to the poor inhibition of **5**. Similar trends were observed in the interaction profiles of

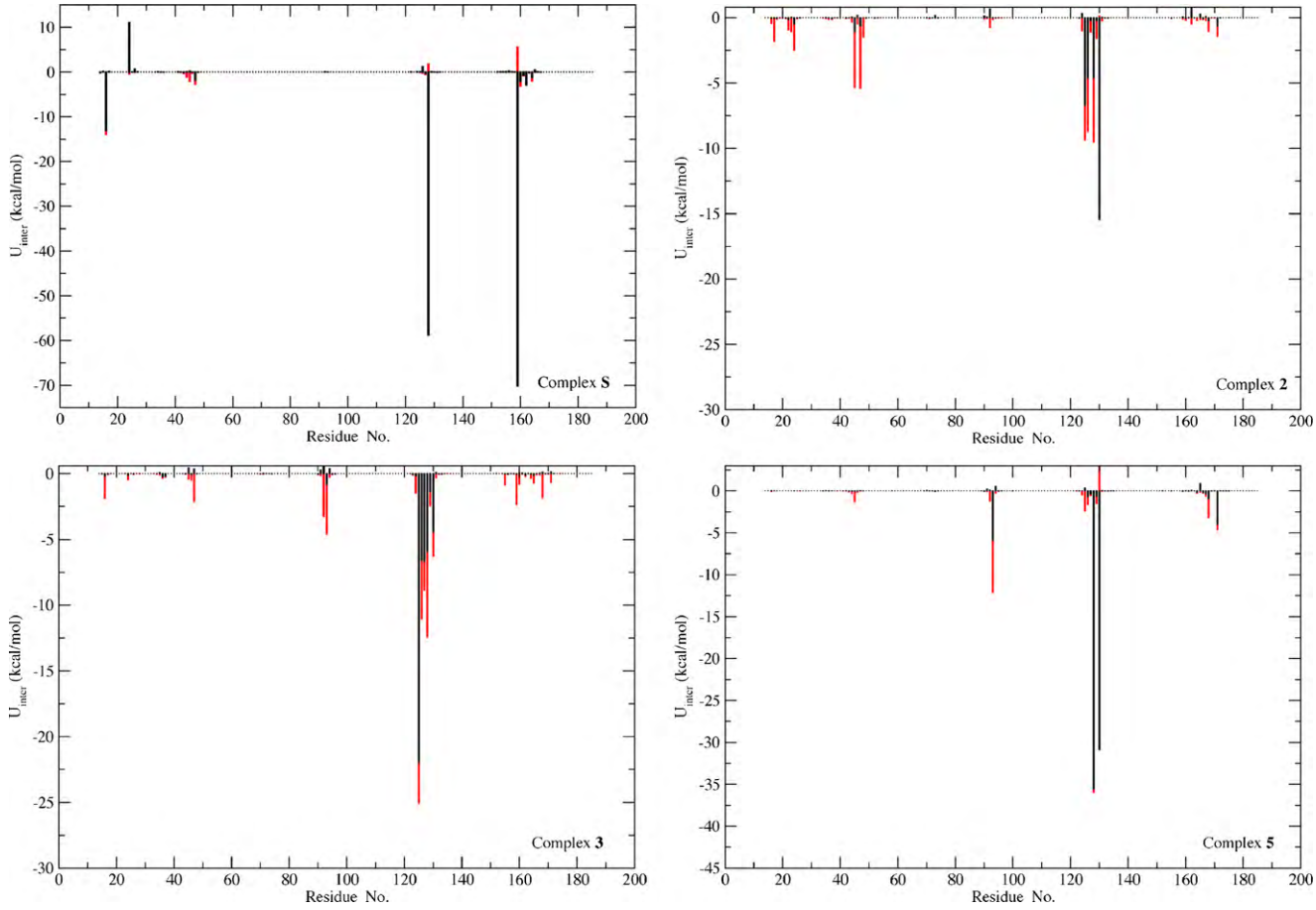

Fig. 7. Average electrostatic (black bars) and non-polar (red bars) interaction energy of the ligands with each residue of the PTEN phosphatase domain in complexes **2**, **3**, **5** and **S**. The interactions were computed between all pairs of atoms. (For interpretation of the references to color in this figure legend, the reader is referred to the web version of the article.)

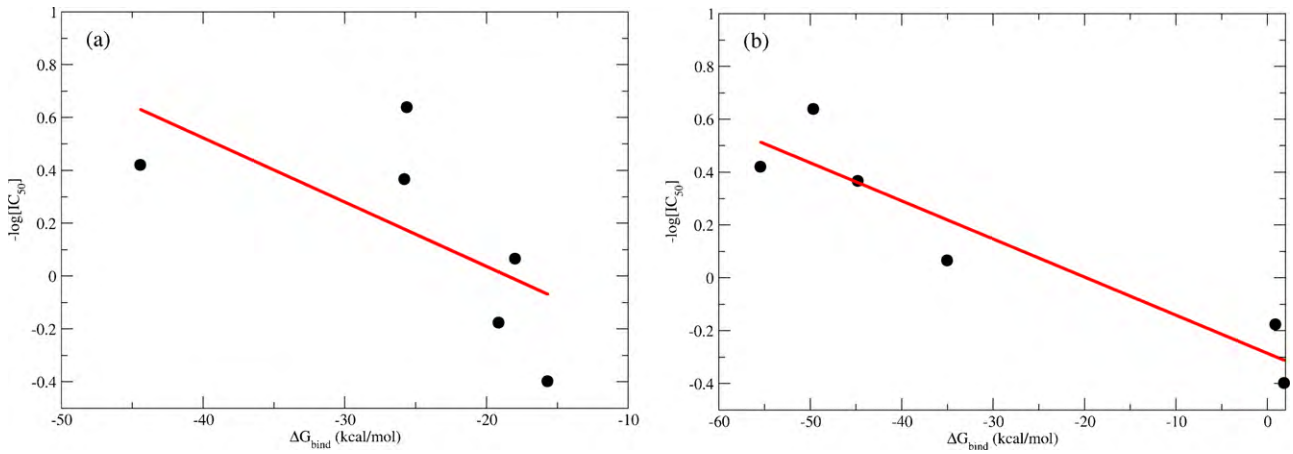

Fig. 8. The binding free energy obtained by MM-GBSA plotted against the binding affinities estimated from the experimentally measured IC_{50} values (black circles) using the original OPLSAA 2001 charges (a) and the reparameterized charges (b). The red lines shows a linear fit with a correlation coefficient $R^2 = 0.419$ (a) and $R^2 = 0.873$ (b). (For interpretation of the references to color in this figure legend, the reader is referred to the web version of the article.)

the remaining D-series and L-series ligands, which are provided as Fig. S4 of the Supporting Information. Notably, in addition to strong hydrogen bonded salt bridge between the phosphate and Lys125, and the hydrogen bonds between the backbone amides of Ala126, Gly127 and Lys128 as well as Arg130 with the inositol hydroxyls, the relatively potent L-series inhibitor **3** also exhibits significant non-polar interactions between the lipid tails and residues 16, 47, 126, 127, 128, 159 and 168 lining the hydrophobic pocket as well as His93.

While interaction energies provide important indicators to the activity of the 3-deoxy-diC_8PI compounds, the inhibition capacity is more closely related to the binding affinity, of which the interaction energies are just one component. Due to relatively large differences in binding modes, particularly between L-series and D-series inhibitors, rigorous calculation of relative binding free energies via free energy perturbation or thermodynamic integration techniques was not feasible. Instead, we utilized a more approximate MM-GBSA approach [46] to obtain an estimate of the contributions from the solvation in addition to the ligand–protein interactions. The results for the six 3-deoxy-diC_8PIs and the substrate are shown in comparison with the measured IC_{50} values in Fig. 8(a), and summarized in Table S1 of the Supporting Information. Overall, the computed binding affinities are in good agreement with experimental data. In particular, the ΔG_{bind} for D-series compounds **2** and **6**, both of which are submillimolar inhibitors, was found to be favorable and comparable to that of the substrate, whereas ΔG_{bind} was ~10 kcal/mol higher for L-series compounds **1** and **5**, both of which exhibited relatively poor inhibition capacity. Interestingly, MM-GBSA predicts the highest binding affinity for the L-series compound **3**, largely due to substantially lower electrostatic desolvation penalty compared to the other ligands. While **3** was shown to be a good inhibitor, it was less effective than compound **2**, and comparable in potency to compound **6**. This result illustrates the limitations of the MM-GBSA method, which tends to overestimate the electrostatic contributions to the binding affinity relative to the hydrophobic effects [47]. Hence, while generally capable of capturing qualitatively the trend in activity of a congeneric series of ligands, the MM-GBSA approach sometimes fails to properly describe the relative binding thermodynamics of specific congeneric pairs [48]. To assess the extent to which these discrepancies can be attributed to force field limitations, we performed density functional theory calculations to refit the partial charges for a single conformation of each of the ligand–protein complexes, since atomic charges are generally the least transferable parameters of fixed charge force fields. Binding free energies were then recomputed using these new charge sets, and the results are shown in comparison with the measured IC_{50} values in Fig. 8(b), and summarized in Table S2 of the Supporting Information.

Clearly, the correlation improved substantially upon reparameterization, indicating that the correct treatment of electrostatics in large, flexible molecules via fixed charge force fields remains a challenge. An additional difficulty is presented in cases where molecular length scale effects, such as displacements of individual water molecules from the confined regions of the protein active site, play an important role in the solvation thermodynamics of the binding event. The free energy released through the displacement of such confined waters from the pβ_2–α_1-P cleft of the PTEN phosphatase domain through the binding of acyl tails of D-series ligands likely comprises a significant portion of their high binding affinity, and this effect is usually not captured by continuum solvation models such as MM-GBSA [49]. Overall, the quality of the MM-GBSA predictions is comparable to recent ligand binding studies using this approach [50–52].

3.4. Experimental validation of modeled complexes

A key feature of the simulations is that there is a different balance of hydrophilic and hydrophobic interactions for the different deoxy-PI compounds binding to PTEN. The relative importance of hydrophobic interactions for the soluble dioctanoyl-PI inhibitors was investigated by enzyme kinetics using long chain dipalmitoyl-PI(3)P as the substrate and solubilizing it with the detergent Triton X-100 in mixed micelles or with 1-palmitoyl-2-oleoyl-phosphatidylcholine (POPC) presented in large unilamellar vesicles (LUVs).

In the mixed micelle assay system (0.1 mM dipalmitoyl-PI(3)P and 0.4 mM TX-100), the large excess of detergent may have two effects. It can enhance solubilization of the deoxy-diC_8PI compounds in micelles (particularly as the inhibitor CMC is approached). However, at low diC_8PI concentrations where the inhibitor is likely to exist as a monomer, the detergent molecules (themselves with a CMC ~0.2 mM) may bind to the protein in the regions suggested by the simulations to harbor the deoxy-PI acyl chains. In either of these cases, the remaining driving force for the short-chain PI analog binding to PTEN would be the polar interactions of the inositol ring. As shown in Fig. 9A, there is little inhibition of PTEN hydrolysis of 0.1 mM dipalmitoyl-PI(3)P, even at concentrations above the CMC of most of the diC_8PI compounds. Only **5** (L-diC_8PI) appears to be a significant inhibitor. In the structures obtained in the simulations, **5** also appears to form the strongest

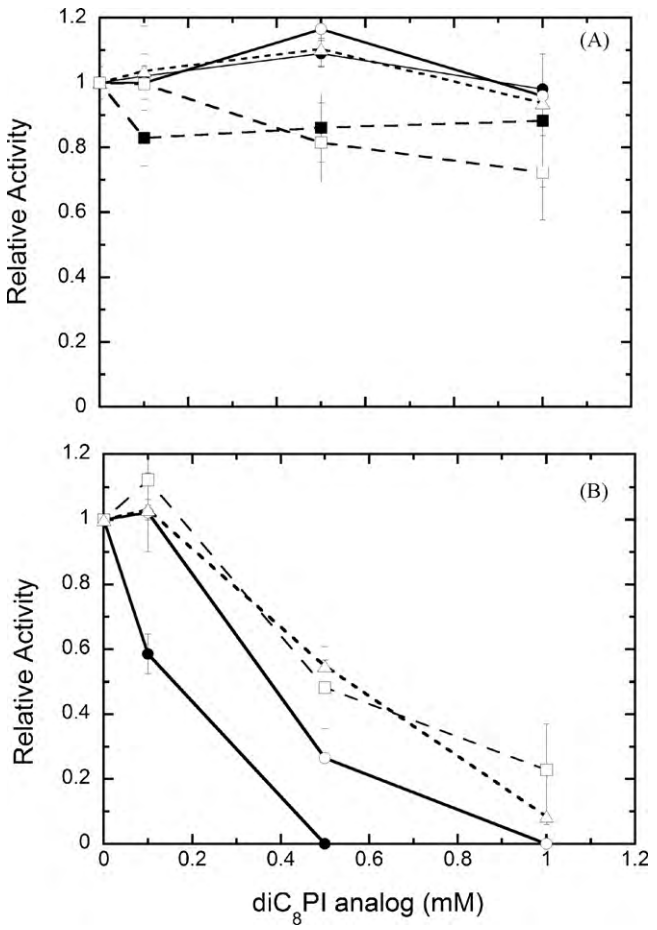

Fig. 9. Effect of different concentrations of diC_8PI compounds on PTEN-catalyzed hydrolysis of 0.1 mM dipalmitoyl-PI(3)P in (A) 0.4 mM Triton X-100 micelles or (B) unilamellar vesicles with 0.9 mM POPC: ●, **2** (D-3-deoxy-diC_8PI); ○, **1**, (L-3-deoxy-diC_8PI); ■, **6** (D-diC_8PI); □, **5** (L-diC_8PI); △, **3** (L-3,5-dideoxy-diC_8PI).

hydrogen bond network with residues in the PTEN active site. The best inhibitor in assays with monomeric **S** (D-$diC_8PI(3)P$) was compound **2** (D-3-deoxy-diC_8PI). However, this compound had the least interactions of the inositol ring with PTEN. It is not an inhibitor in the mixed micelle assay system, consistent with hydrophobic interactions as the dominant forces in the binding of this compound to PTEN.

In contrast to the mixed micelles, PI/PC vesicles are unlikely to present any acyl chain moieties for interaction with PTEN. As long as the diC_8PI compound is below its CMC, it is likely to exist as mostly monomer. Thus, the most potent inhibitor should be **2** (D-3-deoxy-diC_8PI) as seen with the original assays using **S** as the substrate [17]. This is, in fact, what is observed (Fig. 9B). At the CMC and higher concentrations, all the short-chain compounds will be mixed with the vesicles and all are likely to compete with substrate for binding to PTEN. At 0.5 mM or higher diC_8PI compound, all the molecules are inhibitory in this assay system.

One of the unexpected features of the MD simulations was the hydrophobic site formed by the loop containing Arg47. This region is suggested to be a major part of stabilizing the binding of D-diC_8PI compounds and not the L-isomer. We chose to mutate Arg47 to probe the importance of this residue for enzyme activity. D-$diC_8PI(3)P$ at 0.5 mM, where the molecule alone is mostly monomeric [17], was used as the substrate. This should be a good test of the importance of this site for D-enantiomer ligand binding. As shown in Table 2, whether Arg47 is replaced with a glycine, a lysine or a hydrophobic residue, the enzyme specific activity

Table 2
Specific activity of PTEN wild type and single mutants towards the substrate D-$diC_8PI(3)P$.

PTEN	Specific activity (nmol min^{-1} mg^{-1})	Relative activity
Wild type	14.2 ± 0.4	1.000
R47G	0.23 ± 0.03	0.016
R47K	0.082 ± 0.001	0.006
R47L	0.13 ± 0.03	0.009
R47W	0.0046	0.0003

towards D-$diC_8PI(3)P$ decreased significantly. R47W is the worst enzyme (3000-fold poorer), presumably because of the bulky and inflexible nature of the tryptophan side chain. The low activity for the R47K protein was particularly surprising, since the lysine side chain has both the hydrophobic chain and positive charge of the arginine side chain. To assess any protein misfolding, we examined the CD spectra of wild type and R47K PTEN. There was no difference in the far UV spectrum (data not shown) indicating that the bulk of the mutant protein is as folded as normal recombinant PTEN. We cannot easily increase substrate concentration since the aggregation of D-$diC_8PI(3)P$ is likely to complicate kinetics. However, these results clearly show that the interaction of the side chains from this loop region really do contribute to correct substrate binding.

As a further test of the relevance of this hydrophobic site, we examined the potency of L-3,5-dideoxy-diC_8PI as an inhibitor of R47G, the most active of the PTEN mutant proteins. In the simulations, this fairly potent L-isomer does not exploit the region around Arg47 for anchoring its acyl chains. Adding 0.1 mM L-3,5-dideoxy-diC_8PI to substrate (0.5 mM $diC_8PI(3)P$) reduced the specific activity of authentic PTEN to 0.73 of the value in the absence of the L-dideoxy-compound, confirming what was seen previously [17]. The same assay conditions with R47G PTEN led to a more pronounced inhibition – the residual activity of R47G was 0.34 ± 0.04 that in the absence of inhibitor. We can compare this extent of inhibition for R47G PTEN with the published curve for PTEN [17], where 0.5 mM L-3,5-dideoxy-diC_8PI was needed to reduce enzyme activity to one third of the value for substrate alone. Thus, as predicted by the molecular dynamics, the L-isomer is a more potent inhibitor of PTEN when interactions of Arg47 with the D-isomer substrate are precluded, presumably because its acyl chains bind to a different site on the protein.

These kinetic results with short-chain PI inhibitor molecules strongly support the energy minimized complexes obtained from simulations. In each assay system, there is a difference in the ordering of which diC_8PI compound is the most inhibitory. Analyzing inhibitor binding in terms of polar and nonpolar contributions of monomeric PI compounds allows us to rationalize the inhibition observed in three different assay systems where other components modulate how PTEN is affected by these compounds.

4. Conclusions

In this paper we have used molecular modeling and computer simulations to characterize the binding of a series of chiral 3-deoxy-diC_8PI derivatives of the native second messenger ligands, in efforts to explain the experimentally observed variations in the inhibition capacity. A particularly puzzling aspect of the latter was the strong dependence of the inhibition capacity on the chirality of the deoxy-inositol ring. We have shown that, while each of the 3-deoxy-diC_8PI binds with the inositol headgroup inserting into the proposed active site of the PTEN phosphate domain that is occupied by tartrate in the crystal structure, the restrictions imposed by the hydrogen bonding pattern between the inositol hydroxyl groups and various residues of the PTEN P loop, lead to distinct binding

geometries for the L-series and D-series ligands. The primary difference appears to be in orientation of the ligand acyl tails with respect to the protein surface. The potent inhibitors of the D-series were found to bind in a manner similar to the substrate, permitting one or both of their lipophilic tails to occupy a hydrophobic cleft formed by the $p\beta_2$-α_1 and P loops. On the other hand, the L-series ligands bind with their tails oriented in the opposite directions with few good protein contacts and largely exposed to the solvent. The exception is **3**, which forms relatively few head group hydrogen bonds with the active site residues, allowing one of its tails to insert into a deep pocket located next to the active site. Our analysis of protein flexibility shows that complexes with good ligand tail protein contacts show a reduction in fluctuations and stabilization of key regions of the protein. While it may appear that this would lower the binding affinity due to a reduction in entropy, the latter is more than compensated by the improvement in ligand–protein interactions, resulting in a strong correlation between the number of favorable protein-tail contacts and the measured inhibition capacity of deoxy-diC_8PIs. These findings suggest that the lipophilic tails play a critical role in modulating the activity of the ligands. Kinetic data showing variations in activity across the diC_8PI series in assay systems with the substrate presented in detergent micelles or vesicles support this interpretation. The hydrophobically driven tail protein association of the inhibitors would likely be masked by detergent monomers occupying the hydrophobic site on the protein. In contrast, the binding of the soluble inhibitor molecules to PTEN assayed in a vesicle system should be similar to what is seen with soluble substrates as long as the inhibitor is monomer. However, once it is above the CMC, it will insert into vesicles and directly compete with substrate and at slightly higher concentrations may convert vesicles to mixed micelles.

The interaction profiles of the substrate and the six inhibitors clearly demonstrate that in addition to the favorable electrostatic interactions of the inositol hydroxyl and phosphate groups with the active site residues, good inhibitors also display significant nonpolar interactions of the acyl tails with the protein. Interaction energy alone is not sufficient to fully characterize the variation in inhibition potency of the deoxy-diC_8PIs, manifested in the fact that several L-series compounds with strong hydrogen bonding interactions are actually poor inhibitors. The strongly hydrophobic nature of tail protein interactions suggests that solvation effects provide a significant contribution to the binding free energy. Our MM-GBSA calculations confirm this, although the correlation of the predicted binding free energies with the measured IC_{50} values was marginal. Significant improvement was obtained upon quantum mechanical reparameterization of ligand charges, suggesting the discrepancies can partly be attributed to force field limitations. On the other hand, the fact that refitting of the charges alone led to substantial improvement in calculated binding affinities suggests that the predicted binding geometries are largely correct. In addition, continuum models such as MM-GBSA, are known to underestimate contributions to the binding affinity due to hydrophobic desolvation. A more accurate approach based on inhomogenous solvation theory, which treats solvent displacement explicitly on molecular level has been introduced recently [49,53], and will be applied to this problem in a subsequent study.

In addition to identifying the $p\beta_2$–α_1-P cleft as a novel binding site for small molecule PTEN inhibitors, the discovery of a new binding mode for compound **3**, the only potent L-series inhibitor identified thus far, is particularly encouraging, since the favorable tail–protein interactions are attained in a geometry distinct from that of the substrate. Hence, inhibitors based on L-phosphatidylinositols are likely to be more selective towards PTEN than their D-series counterparts which may interact with other second messenger receptors in the 3KI pathway. The implications of this finding will be further explored in a future study.

Acknowledgements

We would like to thank Prof. Scott Miller and Yingju Xu for synthesizing the 3-deoxy-dioctanoylphosphatidylinositol compounds used in this study. This work was supported by a grant from Boston College to G.K. and NIH grant GM60418 to M.F.R.

Appendix A. Supplementary data

Supplementary data associated with this article can be found, in the online version, at doi:10.1016/j.jmgm.2010.05.004.

References

[1] D.M. Li, H. Sun, TEP1, encoded by a candidate tumor suppressor locus, is a novel protein tyrosine phosphatase regulated by transforming growth factor beta, Cancer Res. 57 (1997) 2124–2129.
[2] J. Li, C. Yen, D. Liaw, K. Podsypanina, S. Bose, S.I. Wang, et al., PTEN, a putative protein tyrosine phosphatase gene mutated in human brain, breast, and prostate cancer, Science 275 (1997) 1943–1947.
[3] T. Maehama, J.E. Dixon, The tumor suppressor, PTEN/MMAC1, dephosphorylates the lipid second messenger, phosphatidylinositol 3,4,5-trisphosphate, J. Biol. Chem. 273 (1998) 13375–13378.
[4] M.P. Myers, I. Pass, I.H. Batty, J. Van der Kaay, J.P. Stolarov, B.A. Hemmings, et al., The lipid phosphatase activity of PTEN is critical for its tumor suppressor function, Proc. Natl. Acad. Sci. U.S.A. 95 (1998) 13513–13518.
[5] P.A. Steck, M.A. Pershouse, S.A. Jasser, W.K.A. Yung, H. Lin, A.H. Ligon, et al., Identification of a candidate tumour suppressor gene, MMAC1, at chromosome 10q23.3 that is mutated in multiple advanced cancers, Nat. Genet. 15 (1997) 356–362.
[6] S.F. Barnett, L.M. Ledder, S.M. Stirdivant, J. Ahern, R.R. Conroy, D.C. Heimbrook, Interfacial catalysis by phosphoinositide 3′-hydroxykinase, Biochemistry 34 (1995) 14254–14262.
[7] T. Seufferlein, Novel protein kinases in pancreatic cell growth and cancer, Int. J. Gastrointest. Cancer 31 (2002) 15–21.
[8] I. Vivanco, C.L. Sawyers, The phosphatidylinositol 3-kinase-AKT pathway in human cancer, Nat. Rev. Cancer 2 (2002) 489–501.
[9] P.M. Ghosh, S. Malik, R. Bedolla, J.I. Kreisberg, Akt in prostate cancer: possible role in androgen-independence, Curr. Drug Metab. 4 (2003) 487–496.
[10] D. Kim, H.C. Dan, S. Park, L. Yang, Q.Y. Liu, S. Kaneko, et al., Akt/PKB signaling mechanisms in cancer and chemoresistance, Front. Biosci. 10 (2005) 975–987.
[11] D.P. Stokoe, Curr. Biol. 11 (2001) R502.
[12] K. Du, S. Herzig, R.N. Kulkarni, M. Montminy, TRB3: a tribbles homolog that inhibits Akt/PKB activation by insulin in liver, Science 300 (2003) 1574–1577.
[13] S. Iida, A. Ono, K. Sayama, T. Hamaguchi, H. Fujii, H. Nakajima, et al., Accelerated decline of blood glucose after intravenous glucose injection in a patient with Cowden disease having a heterozygous germline mutation of the PTEN/MMAC1 gene, Anticancer Res. 20 (2000) 1901–1904.
[14] B. Stiles, Y. Wang, A. Stahl, S. Bassilian, W.P. Lee, Y.-J. Kim, et al., Liver-specific deletion of negative regulator Pten results in fatty liver and insulin hypersensitivity, Proc. Natl. Acad. Sci. U.S.A. 101 (2004) 2082–2087.
[15] B.L. Stiles, C. Kuralwalla-Martinez, W. Guo, C. Gregorian, Y. Wang, J. Tian, et al., Selective deletion of Pten in pancreatic {beta} cells leads to increased islet mass and resistance to STZ-induced diabetes, Mol. Cell. Biol. 26 (2006) 2772–2781.
[16] J.P. Lai, B. Shengying, C.D. Ian, L.K. Daren, Inhibition of the phosphatase PTEN protects mice against oleic acid-induced acute lung injury, Br. J. Pharmacol. 156 (2009) 189–200.
[17] Y.K. Wang, W. Chen, D. Blair, M. Pu, Y. Xu, S.J. Miller, et al., Insights into the structural specificity of the cytotoxicity of 3-deoxyphosphatidylinositols, J. Am. Chem. Soc. 130 (2008) 7746–7755.
[18] S.S. Castillo, J. Brognard, P.A. Petukhov, C.Y. Zhang, J. Tsurutani, C.A. Granville, et al., Preferential inhibition of Akt and killing of Akt-dependent cancer cells by rationally designed phosphatidylinositol ether lipid analogues, Cancer Res. 64 (2004) 2782–2792.
[19] R.U. Lemieux, How water provides the impetus for molecular recognition in aqueous solution, Acc. Chem. Res. 29 (1996) 373–380.
[20] Y. Tor, Targeting RNA with small molecules, ChemBioChem 4 (2003) 998–1007.
[21] J.-O. Lee, H. Yang, M.-M. Georgescu, A. Di Cristofano, T. Maehama, Y. Shi, et al., Crystal structure of the PTEN tumor suppressor: implications for its phosphoinositide phosphatase activity and membrane association, Cell 99 (1999) 323–334.
[22] T.L. Andresen, D.M. Skytte, R. Madsen, Synthesis of anti-tumour phosphatidylinositol analogues from glucose by the use of ring-closing olefin metathesis, Org. Biomol. Chem. 2 (2004) 2951–2957.
[23] J.J. Gills, P.A. Dennis, The development of phosphatidylinositol ether lipid analogues as inhibitors of the serine/threonine kinase, Akt, Exp. Opin. Invest. Drugs 13 (2004) 787–797.
[24] A.P. Kozikowski, H. Sun, J. Brognard, P.A. Dennis, Novel PI analogues selectively block activation of the pro-survival serine/threonine kinase Akt, J. Am. Chem. Soc. 125 (2003) 1144–1145.
[25] R.B. Campbell, F.H. Liu, A.H. Ross, Allosteric activation of PTEN phosphatase by phosphatidylinositol 4,5-bisphosphate, J. Biol. Chem. 278 (2003) 33617–33620.

[26] G. McConnachie, I. Pass, S.M. Walker, P.C. Downes, Interfacial kinetic analysis of the tumour suppressor phosphatase. PTEN: evidence for activation by anionic phospholipids, Biochem. J. 371 (2003) 947–955.
[27] H.J.C. Berendsen, D. Vanderspoel, R. Vandrunen, Gromacs—a message-passing parallel molecular-dynamics implementation, Comput. Phys. Commun. 91 (1995) 43–56.
[28] E. Lindahl, B. Hess, D. van der Spoel, GROMACS 3.0: a package for molecular simulation and trajectory analysis, J. Mol. Model. 7 (2001) 306–317.
[29] D. Van der Spoel, E. Lindahl, B. Hess, G. Groenhof, A.E. Mark, H.J.C. Berendsen, GROMACS: fast, flexible, and free, J. Comput. Chem. 26 (2005) 1701–1718.
[30] Maestro, Maestro, Schrodinger, LLC, New York, 2008.
[31] W.L. Jorgensen, D.S. Maxwell, J. TiradoRives, Development and testing of the OPLS all-atom force field on conformational energetics and properties of organic liquids, J. Am. Chem. Soc. 118 (1996) 11225–11236.
[32] G.A. Kaminski, R.A. Friesner, J. Tirado-Rives, W.L. Jorgensen, Evaluation and reparametrization of the OPLS-AA force field for proteins via comparison with accurate quantum chemical calculations on peptides, J. Phys. Chem. B 105 (2001) 6474–6487.
[33] W.L. Jorgensen, J. Chandrasekhar, J.D. Madura, R.W. Impey, M.L. Klein, Comparison of simple potential functions for simulating liquid water, J. Chem. Phys. 79 (1983) 926–935.
[34] U. Essmann, L. Perera, M.L. Berkowitz, T. Darden, H. Lee, L.G. Pedersen, A smooth particle mesh ewald method, J. Chem. Phys. 103 (1995) 8577–8593.
[35] W.G. Hoover, Canonical dynamics—equilibrium phase-space distributions, Phys. Rev. A 31 (1985) 1695–1697.
[36] H.J.C. Berendsen, J.P.M. Postma, W.F. Vangunsteren, A. Dinola, J.R. Haak, Molecular-dynamics with coupling to an external bath, J. Chem. Phys. 81 (1984) 3684–3690.
[37] A. Ghosh, C.S. Rapp, R.A. Friesner, Generalized born model based on a surface integral formulation, J. Phys. Chem. B 102 (1998) 10983–10990.
[38] Prime, Prime, Schrodinger, LLC, New York, 2008.
[39] Jaguar, Jaguar, Schrodinger, LLC, New York, 2008.
[40] S. Das, J.E. Dixon, W. Cho, Membrane-binding and activation mechanism of PTEN, Proc. Natl. Acad. Sci. U.S.A. 100 (2003) 7491–7496.
[41] O.H. Lowry, N.J. Rosebrough, A.L. Farr, R.J. Randall, Protein measurement with the Folin phenol reagent, J. Biol. Chem. 193 (1951) 265–275.
[42] G. Jones, P. Willett, R.C. Glen, A.R. Leach, R. Taylor, Development and validation of a genetic algorithm for flexible docking, J. Mol. Biol. 267 (1997) 727–748.
[43] W. Novak, H. Wang, G. Krilov, Role of protein flexibility in the design of Bcl-XL targeting agents: insight from molecular dynamics, J. Comput. Aided Mol. Des. 23 (2009) 49–61.
[44] F. Mancinelli, M. Caraglia, A. Budillon, A. Abbruzzese, E. Bismuto, Molecular dynamics simulation and automated docking of the pro-apoptotic Bax protein and its complex with a peptide designed from the Bax-binding domain of anti-apoptotic Ku70, J. Cell. Biochem. 99 (2006) 305–318.
[45] S.G. Dastidar, D.P. Lane, C.S. Verma, Multiple peptide conformations give rise to similar binding affinities: molecular simulations of p53-MDM2, J. Am. Chem. Soc. 130 (2008) 13514–13515.
[46] N. Huang, C. Kalyanaraman, K. Bernacki, M.P. Jacobson, Molecular mechanics methods for predicting protein–ligand binding, Phys. Chem. Chem. Phys. 8 (2006) 5166–5177.
[47] G. Holger, A.C. David, Converging free energy estimates: MM–PB(GB)SA studies on the protein–protein complex Ras–Raf, J. Comput. Chem. 25 (2004) 238–250.
[48] B. Kuhn, P. Gerber, T. Schulz-Gasch, M. Stahl, Validation and use of the MM–PBSA approach for drug discovery, J. Med. Chem. 48 (2005) 4040–4048.
[49] R. Abel, T. Young, R. Farid, B.J. Berne, R.A. Friesner, Role of the active-site solvent in the thermodynamics of factor Xa ligand binding, J. Am. Chem. Soc. 130 (2008) 2817–2831.
[50] C.R.W. Guimaraes, M. Cardozo, MM–GB/SA rescoring of docking poses in structure-based lead optimization, J. Chem. Inf. Model. 48 (2008) 958–970.
[51] D.A. Pearlman, Evaluating the molecular mechanics poissonâ' Boltzmann surface area free energy method using a congeneric series of ligands to p38 MAP kinase, J. Med. Chem. 48 (2005) 7796–7807.
[52] A. Weis, K. Katebzadeh, P. Soderhjelm, I. Nilsson, U. Ryde, Ligand affinities predicted with the MM/PBSA method: dependence on the simulation method and the force field, J. Med. Chem. 49 (2006) 6596–6606.
[53] T. Young, R. Abel, B. Kim, B.J. Berne, R.A. Friesner, Motifs for molecular recognition exploiting hydrophobic enclosure in proteinâ€" ligand binding, Proc. Natl. Acad. Sci. U.S.A. 104 (2007) 808–813.